Glass for photonics

Wilfried Blanc, John Ballato, Maurizio Ferrari

Glass for photonics

Wilfried Blanc[1,a], **John Ballato**[2], **Maurizio Ferrari**[3]

[1] Institut de Physique de Nice, CNRS, Université Côte d'Azur, 06200 Nice, France
[2] Department of Materials Science and Engineering, Clemson University, Clemson, SC 29634, USA
[3] IFN-CNR, CSMFO Lab. and FBK Photonics Unit, Via Alla Cascata 56/C, 38123 Povo, Trento, Italy

Abstract In honor of the *International Year of Glass 2022* (IYoG'22), this article highlights important aspects of glass and light, focusing on more advanced photonic applications that drive a great many current and future commercially and societally beneficial products and services. Topics include a brief history of photonic glasses, an overview of light guiding, the subsequent use in planar waveguide devices, and their ubiquity as carriers of information and sensors in the form of optical fibers. These sections highlight the strong interconnections on the understanding of the glass composition, glass structure and optical properties. For next developments in glass photonics, new opportunities will be offered by machine learning, artificial intelligence, 3D printing and additive manufacturing. Additionally, the future of glass photonics may also depend on our ability to meet current challenges such as climate change, i.e., the development of an environmentally-friendly manufacturing process, considering environmental impact and possible material shortages.

1 Introduction and a brief history of glass for photonics

Archeological periods are commonly referred to by the material that represented dominant use or advancement of that time, e.g., the Stone Age, the Copper Age, the Iron Age, etc. Though we stand today in what has been called the Information Age, the ubiquity of information is still predicated on a material—glass—particularly in the form of optical fiber. This point has led some to call today the Glass Age [1].

Of the myriad of historical and modern uses of glass, one that has stood-out for millennia has been its use to shape, transport, and, more generally, employ light. As a result, the history of glass and the history of the use of light are intertwined. From the microscopic to the cosmic, humans have used glass to peer deeper and further into the natural universe. Table 1 provides a summary of milestones in the development and use of glass and light, covering over 6000 years.

Covering the totality of either of these categories, glass and light, let along both, is risibly more than any single article, or book, can properly cover. Accordingly, it is illustrative, especially for the student reader, to summarize some trends in the events of Table 1. Additional details are provided in recent reviews on this topic [2, 3].

One can argue that glass was among the first known materials given its historical origins as a product of the rapid quenching of lava. Its utility as a vessel for containing liquids and food led to its refinement into more sophisticated products, including as art. Approximately concurrent with the advancement of human-made glass, the earliest theories for light and vision were being formulated. By the year 1000, the mathematical underpinnings of optics were quite well developed, and glass was being made in Venice, which was to become the center for artisan glass.

The Middle Ages up through the Renaissance period in Europe begins the era where glass and light come together for specific purposes, particularly for microscopy and astronomy. By the 1800s, particularly based on the partnership between Adolf Winkelmann and Otto Schott, who originated a more scientific approach for engineering the properties of optical glasses, which would be used by Ernst Abbe whose microscope designs were employed by Carl Zeiss [4].

The invention of the maser in the 1950s and the realization of its shorter-wavelength brethren, the laser, in the 1960s represent the beginning of the transition from optics to photonics. With respect to photonics glasses, arguably the 1960s into the 1970s were a transformational decade. During this period, the glass laser (1961 [5]), glass optical fiber amplifier (1964 [6]), the postulation of sub-20-dB/km loss levels in silica optical fibers (1966 [7]), followed by the realization of such (1970 [8]) laid the foundation for what today is the Internet and the (glass-enabled) Information Age.

As a concluding note to this brief history of glass and light, it should be unsurprising that the United Nations celebrated independently, but in rapid succession, the International Year of Light in 2015 and the International Year of Glass in 2022 [9]. The

[a] e-mail: wilfried.blanc@inphyni.cnrs.fr (corresponding author)

Table 1 A brief history of milestones in glass and light

Year	Glass	Light
Stone Age (~ 4000 BC–2000 BC)	First glass known to stone age people (obsidian, volcanic glass)	
3500 BC	Earliest known human-made glass (Egypt and Eastern Mesopotamia)	
400 BC		Plato's "emission theory" of vision: we see because our eyes emit vision beams
399–300 BC	Founding of Alexandria (331) accelerates development of glass production	
300 BC		Euclid writes *Optica*. In it, he proposes that light travels in straight lines and provides mathematical formulae for reflection and refraction
100 BC	Discovery of glassblowing	
160 AD		Ptolemy writes about refraction and further expands the emission theory of vision
982	First recorded reference to Venetian glass-making	
984		Ibn Sahl writes *On burning mirrors and lenses,* which describes how curved mirrors and lenses work. He also discovers a law of refraction equivalent to Snell's law Ibn al-Haytham, (965–1040 AD) writes the *Book of Optics*, a seven-volume treatise on optics. Also develops the Intromissionist theory (1021 AD), which posits that vision occurs because light rays entering the eye. He also proposes that magnification results from refraction and link magnification to glass curvature in lenses
1200–1299	Soda (Na_2O) added instead of potash (variety of potassium compounds), which now makes glass easier to form Venetian glassmaking moved to Murano (1291), due to risk of fire in Venice	
	Earliest known use of (simple) microscopes resulting from more widespread use of glass lenses for eyeglasses	
1268	Earliest recorded comment on use of lenses for optical purposes. Roger Bacon uses glass spheres for magnification. Discovers light reflecting from objects and not being emitted by them	
1450	Cristallo glass invented, a very clear soda glass	
1590–1620	Earliest known examples of compound microscopes, combining an objective lens and an eye-piece. First telescope patent application (Hans Lippershey, 1608). Patent not awarded	
1604	Johannes Kepler describes how light is focused by the eye	
1610	Galileo improves on Lippershey's telescope design and applies it to astronomy Kepler described a more practical telescope based on a convex objective lens and a convex eye-piece	

Table 1 continued

Year	Glass	Light
1615		Willebrord Snellius describes what today is known as *Snell's Law* (though first described in 984 by Ibn Sahl)
1668		Isaac Newton credited with building the first reflector
1644	Giambattista Odierna's *L'occhio della mosca (The Fly's Eye)* provides first detailed account of the microscopic anatomy	
1665–1676	Robert Hooke publishes *Micrographia* (1665). Antonie van Leeuwenhoek achieves 300 times magnification with a single lens microscope. Van Leeuwenhoek reports the existence of micro-organisms (1676)	
1668		Newton expands Gassendi's corpuscular theory that light
1672	Newton uses a prism to demonstrate how white light is comprised of colors	
1673	Lead oxide added to potash glass resulting in clear, heavy glasses, that are ideal for cutting and shaping	
1678		Christiaan Huygens posits that light consists of waves to explain double refraction
1690	Opalescent glass first introduced in Murano	
1704		Isaac Newton publishes *Opticks*
1801		Thomas Young experimentally supports Huygens's wave theory of light
1815		Augustin Fresnel established the theory of light as wave
1842		Jean Daniel Colladon invents the "lighted laminar water fountain" and Jacques Babinet reports on light guiding in bent glass rods, both based on total internal reflection
1846	Carl Zeiss founds his microscope company	
1854		James Clerk Maxwell proposed the "Dynamical Theory of the Electromagnetic Field" and conjectures that light is a transverse electromagnetic wave John Tyndall formulates the ray picture of optical waveguiding
1866	Ernst Abbe is hired by Zeiss and creates new microscope designs that lead to new types of (engineered) glasses	
1880	William Wheeling patents light-pipes used for illumination. Thomas Edisson patents the light bulb	
1888	Roth and Reuss use bent glass rods to illuminate inside the body	
1893	Adolph Winkelmann published on the "law of mixtures" for glass composition and properties creating the foundation of modern glass science Otto Schott works with Zeiss and Abbe and collaborates with Winkelmann to extend the understanding of glass composition and optical properties	
1899		Max Planck's model for black body radiation and the postulation of quanta
1905		Albert Einstein describes the photoelectric effect and establishes that light consists of quanta, later called photons
1900s	Soda-lime glass invented	

Table 1 continued

Year	Glass	Light
1930	Heinrich Lamm first demonstrates imaging using glass bundles	
1933	First television signals optically transmitted using glass rods	
1952	Alastair Pilkington invents the float glass process for large scale production of flat glass	
1953		First maser built by Townes, Gordon, and Zeiger
1954	Abraham Van Heel invents the cladded fiber	
1955	Maurizio Ferrari born (25 June)	
1960		Theodore Maiman demonstrates the first laser
1961	Elias Snitzer reports on the waveguide modes of cylindrical glass waveguides, fabricates a single mode fiber, and demonstrates the first bulk glass laser	
1962		Robert Hall demonstrates the first semiconductor laser
1963	Observation of the dielectric waveguide mode of light propagation in p-n junctions	
1964	Nobel Prize in Physics for the maser/laser principle	
	Snitzer demonstrates the first fiber laser/amplifier	
1966	Kao and Hockham propose that glass fibers could exhibit transmission lower than 20 dB/km	
1969	September 1969 issue of The Bell System Technical Journal devoted to integrated optics and dielectric waveguides	
1970	Corning breaks the “20 dB/km” loss mark	
1970	Theory of prism-film coupler and thin-film light guides	
1972	First Raman fiber amplifier	
1973		First diode end-pumped fiber laser
1974		Wave-mixing observed in optical fiber
1974	Demonstration the first planar glass waveguide laser using Tl^{+} exchange in an Nd-doped borosilicate glass	
1975	Discovery of fluoride glasses	
	First non-experimental fiber-optic link	
1977	First live telephone traffic using optical fiber	
1980	Fabrication of glass planar optical waveguides by sol–gel technology	
1978	Photosensitivity reported in optical fiber	
1986	Erbium-doped fiber amplifier (EDFA) reported	
1988	First operational transatlantic optical fiber cable	
	Experimental realization of double clad fiber lasers though first suggested in 1961	
1989	Demonstration of planar waveguide laser in Nd-doped crystal	
1995	First photonic bandgap optical fiber	
1996	First microstructured optical fiber	
2000	First supercontinuum generation in an optical fiber	
2009	Nobel Prize in Physics for optical fiber communications	
2014	First papers on flexible glass photonics	
2015		United Nations International Year of Light (IYL 2015)
2022	United Nations International Year of Glass (IYoG 2022)	

Sections that follow summarize this union of glass and light in terms of the light guiding (Sect. 2) and uses in planar (Sect. 3) and fiber (Sect. 4) forms.

2 Light guiding in optical fibers

With the development of optical fibers, the guiding of light in glass seems now quite obvious and does not surprise anymore. However, when in 1841, J.D. Colladon observed for the first time the guiding of light in a stream of water (Fig. 1), the physicist from Geneva described this experiment as "one of the most beautiful, and most curious experiments that one can perform in a course on optics" [10]. One can understand this wonder: water, like glass, is a transparent material. Glass in particular has been used for this particular property that characterizes it and gives it its name: its ability to let light pass through, not to trap it. But glass is transparent not invisible. It lets you see through. It is enough to see that light is reflected by the glass or refracted by passing through it to understand that glass and light interact.

In the sixteenth century, Snell and Descartes empirically formulated the law that accounts for the refraction of a light ray when it changes medium (e.g., from glass to air). They showed that by considering the angles of the incident and refracted light rays measured in relation to the normal to the dioptre (at the interface between the two media), the ratio of the sines of the two angles is equal to a constant. This Snell-Descartes law is now expressed as n_1 x sin $i_1 = n_2$ x sin i_2. It introduces the concept of refractive index n, specific to each medium (labeled 1 and 2) and corresponds to the ratio of the speed of light in vacuum vs. the speed of light in the medium considered. Thus, in a glass whose optical index is about 1.5, the speed of light is about 200,000 km/s. The refractive index is also used to assess the amount of light reflected through the Fresnel formula. Still for an index of 1.5, 4% of light is reflected considering a beam perpendicular to the surface. By increasing this refractive index up to 1.8, as in the case of lead glass, the amount of reflected light reaches up to 8%, explaining why crystal glass looks nicer than ordinary glass. Finally, the optical index depends on the wavelength (dispersion relation). Its value decreases when the wavelength increases. Thanks to this property, Sir Isaac Newton was able to observe the rainbow at the exit of the prism illuminated by a solar ray and from this *experimentum crucis* he built a theory of colors and light.

When a beam of light passes from a medium with n = 1.5 to a medium of lower index (n = 1), the Snell-Descartes formula shows that if $i_1 > 41.81°$ then sin i_2 should be greater than 1 which is impossible. The angle of 41.81° is called the critical angle. For any angle less than this critical angle, the light is partly refracted and partly reflected at the interface. For any angle greater than this critical angle, the light is entirely reflected at the interface. No ray of light is transmitted into the air. This is the phenomenon of total internal reflection (TIR). It exists only for light going from a medium of high index to a medium of lower index. Conversely, a light ray can always penetrate a homogeneous medium of higher index. Thanks to this TIR mechanism, the light can be trapped in the glass by propagating by successive bounces at the interfaces (Fig. 2a). If the reflection is only partial at each bounce, the light can propagate but with a loss of intensity.

It is by this approach, called ray optics, that the guidance of light is generally presented because it requires only one simple formula (that of Snell-Descartes). It allows us to understand the importance of refractive indices or phenomena such as modal dispersion: given the width of the core (where the light propagates), several ray paths can be taken by the light with different angles of reflection. Each of these paths is called a mode of propagation. When a pulse of light enters the fiber and its intensity is shared between the different modes, it will result in a temporal broadening of the pulse, which is detrimental to the information rate due to the possible overlap between each pulse. But beyond the pedagogical interest, this approach based on geometrical optics is no longer valid in the case of optical fibers. The assumption of geometrical optics is that the wavelength of light is very small compared

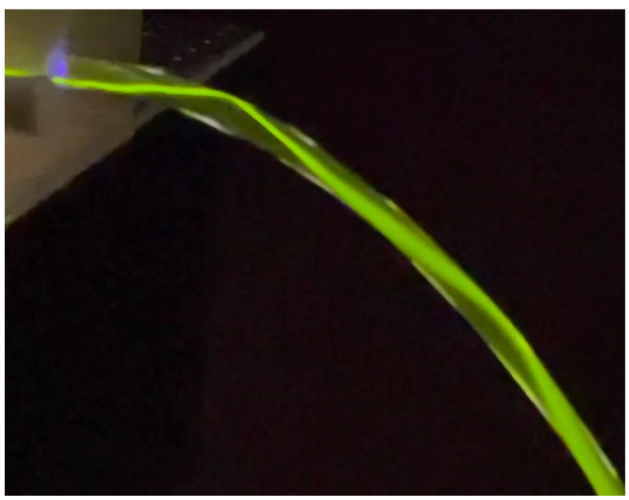

Fig. 1 Laser beam reflected in a water jet at the interface with air. The blue laser is converted into yellow ray due to the rhodamine dissolved in the water

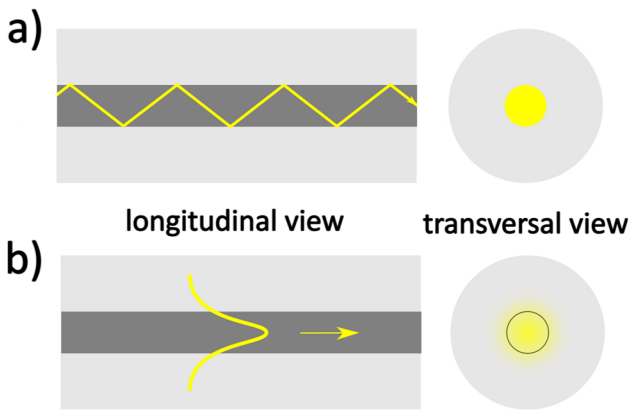

Fig. 2 Illustrations of **a** the Total internal reflection and **b** modal approach of light guiding mechanisms considered in optical waveguides such as optical fibers. Light and dark gray regions correspond to the cladding and the core, respectively. In the transversal view of **b**, the core is delimited by the black circle

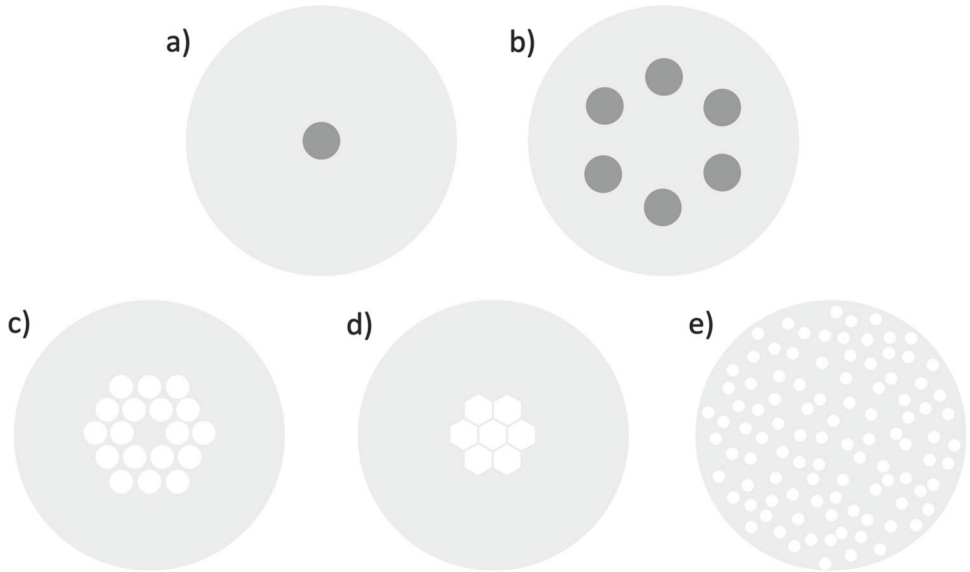

Fig. 3 Schematics of different optical fiber geometries: **a** conventional core-clad fiber, **b** multicore fiber, **c** microstructured fiber, **d** hollow core photonic crystal fiber, **e** transverse Anderson localization fiber. Light gray, dark gray and white colors correspond to silica, glass with higher refractive index than silica (typically germanium doped silica) and air (or glass with lower refractive index than silica), respectively

to the size of the object in which it propagates. In the case of optical fibers, the diameter of the core is about 10 μm, so close to the wavelength of light. The propagation of light in a waveguide is therefore solved using the four Maxwell equations describing the propagation of electromagnetic fields [11]. Each mode of light propagation is then defined with respect to its intensity distribution along a transverse section (Fig. 2b). The light remains confined in the core provided that it has a higher index than the surrounding cladding. However, contrary to the case of ray optics which trapped the light only inside the core, the light is now partially confined in the core, part of the mode propagating in the cladding. This approach being based on the equations of electromagnetic waves, it obviously applies to visible and infrared light generally used in optical fibers (the lowest attenuation of silica is reported at a wavelength of 1.55 μm) but also to THz waves for which optical fibers are also developed [12].

The guiding mode based on a core of higher index than the cladding is the most commonly used. In the case of silica fibers, the increase in the refractive index of the core can be obtained for example by doping the silica with germanium (case of *telecom* fibers, Fig. 3a). This conventional core-clad geometry is now extended to prepare optical fibers containing several cores (Fig. 3b) in order to increase the bandwidth of the fibers. Another approach to maintain the refractive index difference between the core and the cladding relies on keeping a silica core but decreasing the index of the cladding, for example by introducing fluorine or by including air holes (case of micro-structured fibers, Fig. 3c) [13]. A periodic arrangement of these holes makes it possible to carry out a photonic crystal which has the characteristic not to be able to propagate certain wavelengths [14]. Thus, such a wavelength can be propagated in a hollow core crystal photonic fiber, i.e., in a core whose refractive index is lower than that of the cladding, because it is reflected by the photonic structure of the cladding (Fig. 3d). Finally, another type of propagation exists, based on transverse Anderson localization (Fig. 3e) [15]. Such fibers have a transverse cross section containing a random variation of the refractive index but this cross section is longitudinally invariant [16]. For instance, such a fiber can be obtained by forming a bundle, mixing two polymer fibers of different refractive index. If the distance between the heterogeneities is of the order of the light wavelength, the light can be trapped between these heterogeneities by an Anderson localization mechanism, and this all the more as the difference in refractive index is high.

3 Photonic glass planar waveguides

Planar optical waveguides are the critical base of integrated photonics because of the different functionalities concerning the operation necessary to manipulate, generate and detect the optical signals. There is a huge of waveguiding systems, mainly exploiting semiconductor materials, that are employed for lasers diode, optical amplifiers and sensors fabrications but the main drawback is the rare earth doping of such materials. There are a lot of papers in literature presenting different doping techniques of rare earth ions in silicon and other classical semiconductors but the results, although interesting from a scientific point of view, are negligible for applications [17]. It is worthy to note that the Yasufumi Fujiwara group has open the doors to rare-earth activated semiconductors [18]. Fujiwara and coworkers developed the semiconductors intra-center photonics. This novel photonics uses the intra-4f shell transitions of rare-earth ions doped semiconductors. In 2009 Fujiwara invented a narrow-band red LED using Eu-doped GaN (GaN:Eu) and very recently he demonstrated monolithic integration of vertically stacked RGB LEDs composed of GaN:Eu and InGaN quantum wells on the same sapphire substrate [18]. The next step could be the waveguiding configuration on hybrid platform [19].

As a matter of fact, the problem of rare earth doping has been solved by glass photonics as clearly demonstrated by the numerous successful applications of silica-based fibers activated by rare earth ion [20, 21]. In the case of planar waveguides the technical aspect is complicated by the different fabrication technologies and to the high rare earth concentration required in short-length planar structures [22]. Several techniques are currently employed to fabricate photonic planar waveguides, among them RF-sputtering, sol–gel, laser micromachining, ion-exchange, Plasma Enhanced Chemical Vapor Depositions (PECVD) [17]. The solubility of rare earth ions in glass matrix is a very crucial point, especially for silicate based planar waveguides which have a rare earth ions solubility of about 6×10^{20} cm^{-3}. The main factors affecting the performance of glass-based photonics waveguides activated by rare earth ions are: (1) the luminescence quenching induced by the active ion concentration, (2) the efficiency of the pumping scheme, and (3) channel and grating writing. The luminescence quenching has been successfully alleviated by the sol gel technology [9, 23, 24] but the real breakthrough has been the development of transparent waveguiding glass ceramics [25]. In fact, photonic glass–ceramics are strategic because they combine the optical and glass-manufacturing processing properties of the amorphous phase and the single-crystal-like optical and spectroscopic properties of the crystalline phases [25, 26].

The more significant results, based on sol–gel technology, has been obtained for the rare-earth-activated SiO_2–HfO_2 and SiO_2–SnO_2 planar waveguides [27]. Starting from the demonstration of silica-hafnia system as a suitable system for photonics [28, 29] a lot of papers have been published on the subject, including specific applications in integrated optics as the monolithic tapered rib waveguide laser made of Nd^{3+} doped silica hafnia sol–gel, developed for lab-on-a-chip applications [30]. The device is presented in Fig. 4 [26]. This paper is important also because it puts in evidence the technical difficulty in using CHF_3 Reactive Ion Etching (RIE) for rib waveguide and gratings fabrication on sol–gel platform. The authors resolved the problem controlling a complex process where RIE is coupled to photolithography and electron beam lithography [30].

The more important role of hafnia based waveguide glasses and glass–ceramics is the mitigation of the ion-ion interaction among rare earth ions. This is due to the fact that a disruption of the silica network is promoted by HfO_2, Hf^{4+} increases the number of non-bridging oxygen atoms. This allows the matrix to accommodate a high content of rare earth strongly reducing the physical clustering. Moreover, as shown in Fig. 5, the chemical clustering is completely eliminated [24–26].

Looking at the development of sol–gel waveguides glass ceramics, the structures based on SnO_2 nanocrystals have demonstrated to be the most effective. SnO_2 has two unique characteristics, crucial for photonics waveguides: (1) luminescence sensitizing and (2) photorefractivity. These features give solution to the low absorption cross section of the rare-earth ions and to the writing of channels and mirrors in the case of waveguide integrated laser, as mentioned before. The role of SnO_2 nanocrystals as rare-earth ion luminescence sensitizers allows to overcome the low absorption cross section of the Er^{3+} ion [31].

SnO_2 nanocrystals present a high absorption cross section in the UV at around 340 nm corresponding to the SnO_2 interband transition [32], resonant with the electronic levels of several rare earth trivalent ions. Thank to that, in rare earth activated SiO_2–SnO_2 glass–ceramics waveguide, efficient rare earth luminescence enhancement has been demonstrated via energy transfer from host SnO_2

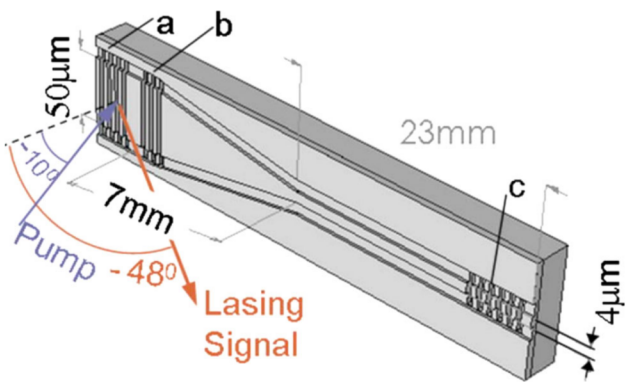

Fig. 4 Schematic view of the $Nd.^{3+}$ doped sol–gel tapered rib waveguide laser based on silica-hafnia sol–gel platform. **a** Input–output grating coupler, **b** partial reflection grating, and **c** total reflection grating. Reproduced with permission from [26]

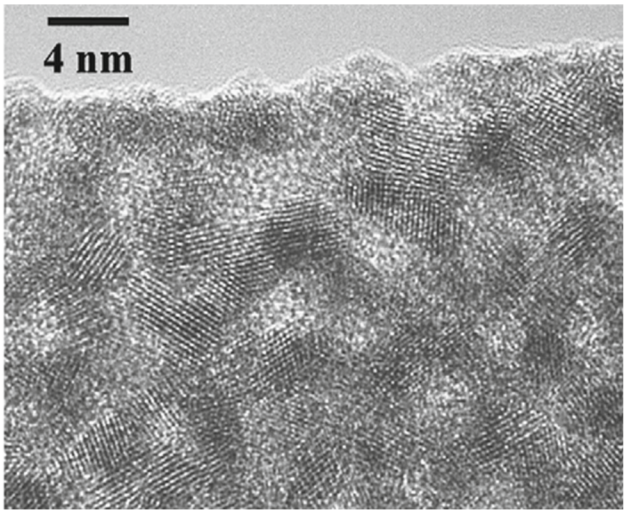

Fig. 5 HRTEM image of the $70SiO_2$-$30HfO_2$ glass ceramic planar waveguide, activated by Er^{3+}ions, showing HfO_2 nanocrystals homogeneously dispersed in the amorphous matrix. Single domain nanocrystals are clearly evidenced. Reproduced with permission from [26]

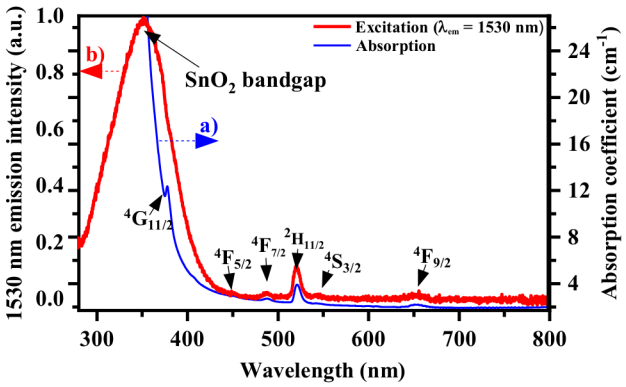

Fig. 6 **a** Room temperature absorption spectrum (blue line) and **b** room temperature excitation spectrum (red line) obtained by detecting at 1530 nm emission of a silica-tin oxide glass–ceramic activated by Er^{3+} ions. Reproduced with permission from [27]

nanocrystals to the rare-earth ions [9, 27, 31, 32]. The role of SnO_2 as an effective rare earth ion luminescence sensitizer is evident from Fig. 6. Figure 6a (blue color) shows the absorption spectrum in the UV–Vis region of the SiO_2–SnO_2 bulk activated by Er^{3+} ions. The band at 340 nm associated to the SnO_2 nanocrystal interband transition, exhibits a much higher intensity than the absorption bands corresponding to the transitions of Er^{3+} from the ground state to the excited states. The sensitizing effect is clearly demonstrated by the 1530 nm excitation spectrum, shown in Fig. 6b (red color). The emission intensity at 1530 nm is extremely high under excitation at 340 nm, when compared with the intensities obtained upon direct excitation in the Er^{3+}electronic states.

The photorefractivity of sol–gel derived SnO_2 glass–ceramics, SiO_2–SnO_2 glass–ceramics exhibit high photorefractivity with negative refractive index changes in the order of 10^{-3}, allows the use of direct laser photoinscription technique to fabricate Bragg gratings and channel waveguides [27, 32]. Figure 7 shows an optical gratings fabricated by a CW frequency doubled argon laser $\lambda =$ 244 nm with a writing fluence of 1.0 kJ/cm^2 on a 4×4 mm^2 area of the $70SiO_2$–$30SnO_2$:$0.5Er^{3+}$ glass–ceramic planar waveguide.

This important demonstration paves the way to the intense use of direct UV writing technique for low-cost and high efficient phototonic planar waveguides fabrication. Of course there is a lot to discuss about glass-based photonics waveguides. To go deeper in the argument we refer the reader to [9, 17] end references herein.

Finally, to close this section is useful to mention the exciting new field of flexible glass photonics where the waveguides are fabricated on flexible substrates. Flexible photonics is an expanding field due to the expected killer applications. In this field glass waveguides are playing a significant role supported by the high-scale industrialization of ultra-thin glasses with thicknesses ranging from tens to hundreds of microns. An exhaustive collection of papers, reflecting the state of art in the field, is given in [33].

4 Photonic glass optical fibers

4.1 The quest of ultratransparent optical fibers

Driven by applications, optical fibers have constantly reinvented themselves to push back their limits. Core-cladding geometry, for example, was first developed in response to a limitation in the use of optical fibers in fiberscope [34, 35]. The use of single-index fibers led to problems of cross-talk between the different fibers when they touched, to the detriment of image quality. Surrounding

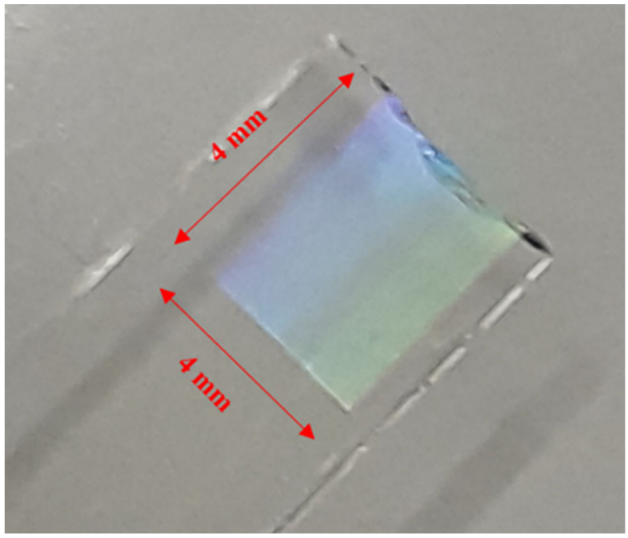

Fig. 7 Optical gratings fabricated by a CW frequency doubled argon laser $\lambda = 244$ nm with a writing fluence of 1.0 kJ/cm^2 on a 4 × 4 mm^2 area of the $70SiO_2$–$30SnO_2$:$0.5Er^{3+}$ glass–ceramic planar waveguide. One can see the colors due to the interference patterns scattering from the gratings based on the Bragg law. (Reproduced from [9] under the terms of the Open Access Publishing Agreement)

the core with a glass cladding improved the quality of the images transmitted. Fiberscopes are therefore important for optical fibers, as they were one of the very first applications and led to the core-cladding structure used for telecom fibers, for example. The glass used at the time had losses of the order of dB/m (1% of light transmitted after 20 m), which was compatible with an application for fiberscope. However, in the 1960s, when new solutions for transporting information were being sought for telecommunications, such losses were an obstacle to the use of optical fibers, since they required signal re-amplification every 20 m. In 1966, CK Kao (Nobel Prize in Physics 2009) and G Hockham published a seminal paper in which they showed that optical losses were extrinsic in nature (e.g., presence of Fe) [7]. They predicted that if a new manufacturing process could overcome these contaminations and achieve a loss of 20 dB/km (1% of light transmitted after 1 km), optical fibers could be used for telecommunications. This first transparent fiber was reported as early as 1970 by a Corning team [8]. It was also in 1970 that the first continuous emission laser diode operating at room temperature was discovered by Z. Alferov (Nobel Prize in Physics in 2000), an indispensable component as a light source for optical fibers [36]. At the end of the 1970s, fiber transparency reached 0.2 dB/km (1% of light transmitted after 100 km). These advances enabled light to travel 5,000 times farther in an optical fiber! The exceptional level of transparency achieved by silica glass, and the boom in telecommunications (Internet, etc.) made possible by such fibers, have helped to make optical fibers one of the 7th Glass Wonders in 2022 [37]. The next sections focus on the transparency of the optical fibers. We encourage those interested in the History of optical fiber to read Refs. [38, 39].

Such an increase in transparency has been made possible thanks to the development of specific manufacturing processes. The manufacture of silica glass (SiO_2) by melt-quenching involves melting sand in a crucible. The resulting glass may therefore be contaminated, due to the initial quality of the sand and possible contamination by the crucible. To avoid such contamination, the Corning team has exploited an initially developed process to prepare silica soot for easier shaping of glass objects. The basic principle of this chemical vapor synthesis consists in reacting a gaseous stream of O_2 and $SiCl_4$ at high temperature (usually using a blowtorch), leading to the formation of silica soot and gaseous Cl_2. This synthesis results in a very high-purity glass, as the liquid $SiCl_4$ (from which the gaseous $SiCl_4$ is derived) is prepared with very high purity, and its vapor pressure is much higher than that of other elements (impurities) that may be present in trace amounts. For example, the vapor pressure of Fe_2Cl_6 is 11 orders of magnitude lower. The three main methods derived from CVD are Outside Vapor Deposition (OVD), Vapor Axial Deposition (VAD) and Modified Chemical Vapor Deposition (MCVD) (Fig. 8) [40]. OVD consists of depositing soot on a rotating mandrel and growing the layers from the inside out, depositing the core layers first. In the case of VAD, simultaneous core and cladding growth is carried out according to the cross section of the preform, with one torch dedicated to core composition and one to cladding. Finally, the MCVD process is based on the deposition of core layers inside a silica tube, which is then collapsed to form a preform (typical diameter: 1 cm, length: 50 cm) that will be drawn into an optical fiber. This latter process is mainly used in industry to prepare specialty optical fibers (i.e., non-telecom fibers). In the case of telecom fibers, the increase in core refractive index was initially obtained by doping with Ti, but the difficulties encountered in stabilizing its oxidation state (leading to light absorption) subsequently led to the use of germanium. Only a few elements can be supplied by the vapor phase (typically Ge, P, F, B). Other elements, such as Al and rare-earth ions, are added by solution doping of the porous core layer.

The development of such high-tech processes has been made possible by the limited quantity of glass required for an optical fiber (125 μm in diameter). It is estimated that just over 400 fiber optic submarine cables are currently laid, for a total length of 1.4 million km. This corresponds to a glass volume of 17.2 m^3 (a cube with a edge of 2.6 m). Considering silica density alone, the total mass of optical fibers laid in submarine cables corresponds to “only” 38 tons, whereas a flame furnace for the glass industry can produce up to 1000 t of glass per day.

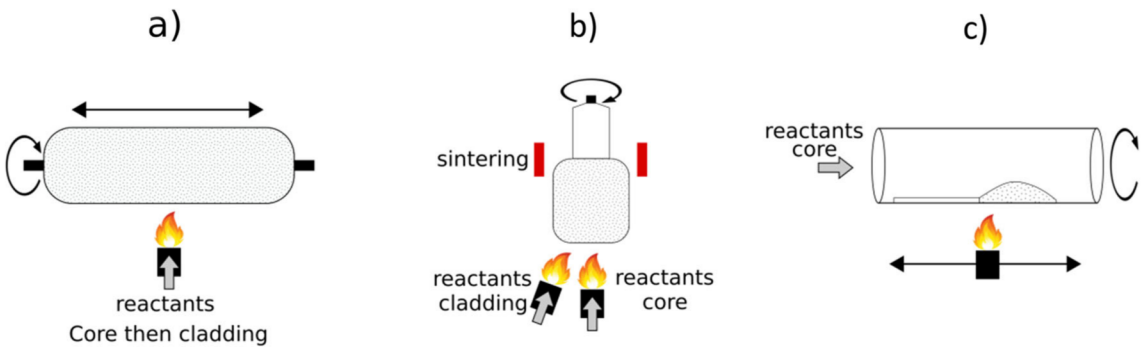

Fig. 8 Schematic diagrams of the **a** outside vapor deposition (OVD), **b** vapor axial deposition (VAD) and **c** modified chemical vapor deposition (MCVD) methods. Dashed areas correspond to soot. Reactants can be $SiCl_4$, $GeCl_4$, O_2, etc. Upper part of the VAD method and layer on the left of the burner in the MCVD method correspond to consolidated soot (i.e., glass bulk or layer)

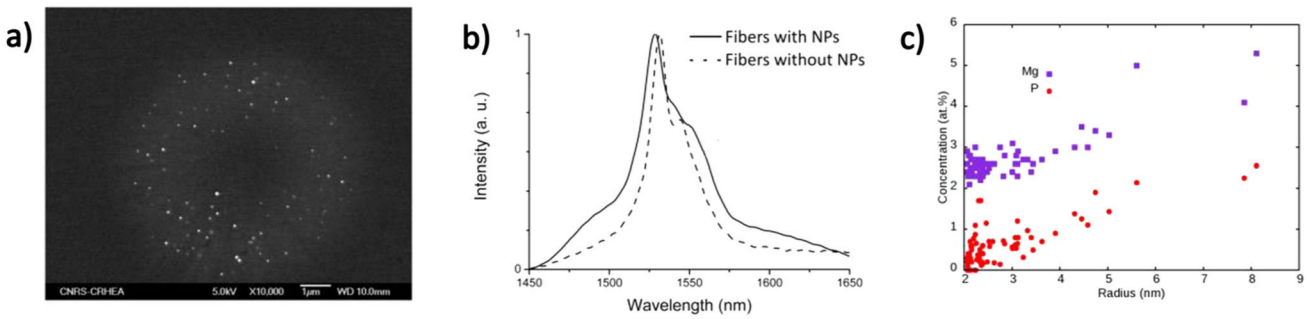

Fig. 9 Optical fibers with nanoparticles (NPs) formed by introducing Mg. **a** SEM image of the fiber core, **b** Er^{3+} emission spectra and **c** variation of the composition of smaller NPs measured by Atom Probe Tomography (Adapted with permission from Ref. 60. Copyright 2019, American Chemical Society)

Elimination of contaminants such as Fe and then OH radicals has resulted in a silica-based optical fiber with a minimum attenuation of 0.2 dB/km, at a wavelength of 1.55 μm. This transmission is mainly limited by the slight compositional and density heterogeneities present in Ge-doped silica glass, inducing Rayleigh light scattering. In order to push back this attenuation limit, the approach is now to prepare a silica-only core, surrounded by a lower-index ring (fluorine-doped silica) to meet the conditions for total internal reflection guidance. Particular attention is paid to the drawing temperature and quenching undergone by the fiber as it leaves the drawing furnace, to give the glass time to relax to its least disordered state, and to limit density fluctuations. The lowest attenuation thus reported is 0.14 dB/km in 2018 [41]. While the 1970s brought attenuation down from 1000 to 0.2 dB/km, the gain over the following forty years may seem small. But it's still important, because by reducing losses from 0.2 to 0.14 dB/km, this corresponds to a 40% improvement in transparency (1% of light transmitted after 143 km), which means that the number of amplifiers can be significantly reduced on a transoceanic line, and therefore represents a significant gain in reliability and economy. Is it possible to be even more transparent? A significant gain in transparency is expected with fluoride fibers, which have a theoretical attenuation 10–100 times lower than that of silica. To date, fluoride fibers have shown higher attenuations than silica-based fibers [42, 43]. However, very encouraging results have been obtained by drawing the fibers in micro-gravity, in space [44]. The measured losses of these fibers approach those expected theoretically, and such transparency could make it possible to envisage a transatlantic link without an amplifier when long length fiber will be prepared.

4.2 Nanoparticles in optical fibers

As highlighted in the previous sections, transparency of optical fiber is a great concern. Several fabrication processes were developed to decrease the presence of extrinsic and intrinsic heterogeneities in the core inducing attenuation by absorption and light scattering. In contrast to this trend, another approach has been initiated through the presence of heterogeneities such as air bubbles or nanoparticles in the core of optical fibers (Fig. 9a). Air bubbles were mainly introduced to induce light scattering for applications in lighting [45]. In this section we will focus on oxide nanoparticles [9, 46, 47].

The presence of oxide nanoparticles was first sought to modify the luminescence properties of rare-earth and transition metal ions. The luminescence properties of these ions are linked to radiative de-excitation among their electronic energy levels [48]. The position of these energy levels depends on the chemical composition and nature (crystalline or glassy) of the atomic environment. For example, in a crystal, all environments are identical and the emission spectrum is characterized by emission lines. In a glass,

the ions have different environments, which contributes to shifting the energy levels. The emission spectrum is then a broad band resulting from the convolution of emission lines from different environments. A change in the chemical environment also leads to a shift in energy levels, and hence a change in emission properties (e.g., emission bandwidth, absorption and emission cross-sections, fluorescence lifetime). Control of the luminescent ion environment is therefore of prime importance. However, not all materials can be drawn into optical fibers. Insertion of nanoparticles in optical fibers thus aims to combine the advantage of manufacturing a silica fiber with the insertion of luminescent ions in nanoparticles of different composition and structure from silica, adapted to the desired luminescence properties. A broadening of the Er^{3+} emission band at 1.55 μm has been demonstrated thanks to the presence of nanoparticles in the fibers (Fig. 9b) [49]. Another benefit of inserting rare-earth ions into nanoparticles is to bring them closer together, thereby promoting energy transfer [50]. Finally, by modifying the chemical environment, the phonon energy can be lowered locally, thereby reducing the probability of non-radiative de-excitations [51, 52]. Given the possibility of controlling luminescence properties, the first applications involved the production of fiber lasers and amplifiers for both rare earth ions and transition metals [53–55]. For instance, when LuF_3:Ho^{3+} nanoparticles were used as precursors, slope efficiency of the 2.1 μm emission was as high as 85% [56]. However, the development of these components remains limited by the light scattering generated by the presence of nanoparticles. Indeed, nanoparticles have a refractive index different from that of the host glass matrix, and therefore behave as light scatterers. Four criteria have been suggested for minimizing light-scattering losses [57]: 1. Particle size must be less than 15 nm; 2. Interparticle spacing must be comparable with the crystal size; 3. Particle-size distribution must be narrow; 4. There cannot be any clustering of the crystals. Additionally, the refractive index difference between the host glass and the nanoparticles must be minimized. For instance, it has been reported that such refractive index difference must be smaller than 0.3 [58]. Lastly, the volume fraction of nanoparticles can be decisive, as above 10% for monodisperse nanoparticles, the optical losses induced by light scattering decrease [59]. However, it is still very difficult to control all these parameters, and optical losses remain an obstacle to the development of lasers and amplifiers. Moreover, according to previous established criteria, nanoparticle size must be minimized. However, it has been shown that the composition of amorphous particles formed by phase separation evolves with their size (Fig. 9c) [60, 61]. The composition of the smallest particles is very similar to that of silica, and deviates from this composition as their diameter increases. This calls into question the added value of the smallest particles, and leads to the need to find a compromise on the size of these particles, which must be small to limit optical losses but large enough to have a modified composition. Furthermore, the change in composition as a function of size implies that light scattering models should consider a variation in refractive index as a function of particle size, and not a single refractive index for all particles, as is currently the case.

While light scattering must be minimized for laser and amplifier applications, in 2018 it began to be exploited for sensor applications [62]. The first measurement techniques were based on frequency-based methods such as Optical Backscatter reflectometry (OBR) (Fig. 10). This technique enables the fiber to be probed over ten or hundreds of meters with a spatial resolution of 10 μm. The ability to detect and localize physical (temperature, stress, etc.) or biological parameters along the entire length of the fiber means that architectures based on hundreds of sensors can be developed, offering real-time 3D detection [63]. This approach has been applied for biophysical sensing. For instance, during thermal ablation of cancer, this multi-fiber architecture was employed to measure steep spatial and temporal gradients of temperature (Fig. 10a) [64–66]. The strain sensitivity of these fibers was exploited to provide 3D shape deformation of medical device such as needles (Fig. 10b and c) [67, 68]. A biosensor can be obtained by biofunctionalizing the surface of the fiber. To improve the sensitivity of the biosensor, the optical cladding is etched to increase the interaction between the light propagating into the core and the bioreceptors [69, 70]. Finally, the detection of ionizing radiation (X-ray) has been reported with these fibers, demonstrating a radiation sensitivity ten times larger than a standard Single Mode Fiber [71]. Another detection protocol has been developed, based on transmission-reflection analysis (TRA) [72, 73]. This alternative relies on the analysis of the transmitted and backscattered emission intensity ratio to locate the point on the fiber subjected to a disturbance. Spatial resolution (a few millimeters) is not as good as with OBR detection, but this method is simpler and cheaper as it necessitates incoherent light source. In addition, the use of artificial intelligence has improved the detection capability of this method by detecting several disturbances simultaneously [74]. A final example of an application based on nanoparticle-induced light scattering concerns the refinement of laser lines [75]. A self-injection locked fiber laser was proposed, based on a hybrid cavity containing nanoparticles doped optical fiber. This scheme allows to achieve a fiber laser with 3 dB linewidth compressed from 16 kHz to 497 Hz. This fiber laser was then amplified to more than 1 W (Fig. 11).

To fabricate core-cladding optical fibers containing nanoparticles, three routes have been explored to date. We now present them briefly. Further details can be found in Refs. [9, 46, 47].

The first process developed to obtain NPs-doped fiber was based on the one used for glass–ceramics: the fiber, initially homogeneous in composition (i.e., without NPs), is heated to form NPs via the nucleation/growth process. This approach has made it possible to form fluoride or oxide particles in a silica-based optical fiber [53–55]. The choice of temperatures (up to 850 °C) and heat treatment duration (several hours) allow the NPs size to be controlled. But this process has its shortcomings: it lasts long, the entire fiber is heated at high temperature which mechanically weakens it due to the crystallization of the optical cladding and the fiber length is limited to the dimension of the oven. Moreover, it is necessary to remove the protective resin cladding around the fiber and then to recoat the fiber.

A second route is based on doping with nanoparticles. The NPs are then dispersed in a liquid (water, ethanol, etc.) and introduced into the core of the preform by impregnation of the porous layer deposited by MCVD. By analogy with the solution doping, this step could be called “suspension doping” as the doping solution is a suspension. This approach was first explored with alumina (Al_2O_3)

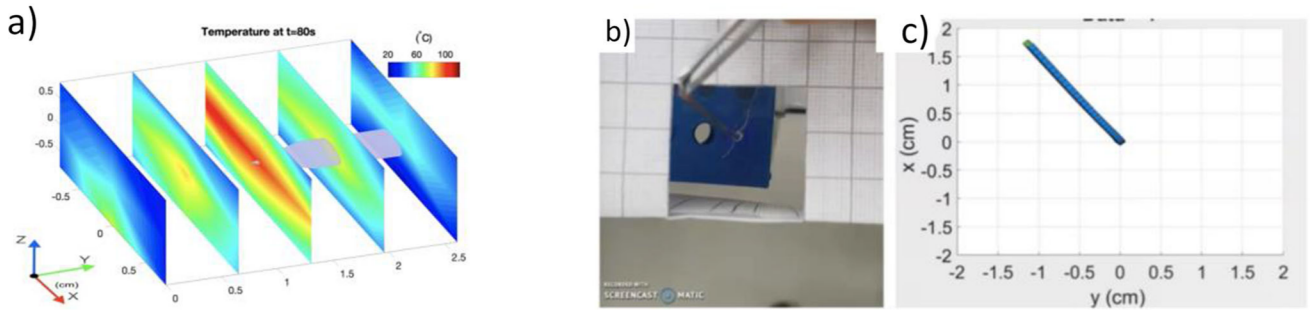

Fig. 10 Applications of NPs-doped fibers used as sensors based on OBR measurements. **a** 3D temperature map, obtained by 12 Nps-doped fibers over a 16 × 16 surface during microwave ablation heating; each plane shows the temperature recorded on the plane perpendicular to the fiber; Real-time sensing, showing the applied deformation (**b**) and its corresponding shape estimation (**c**) Images reproduced from Ref. [64] (**a**) and adapted from Ref. [68] (**b**, **c**) under the terms of the Open Access Publishing Agreement

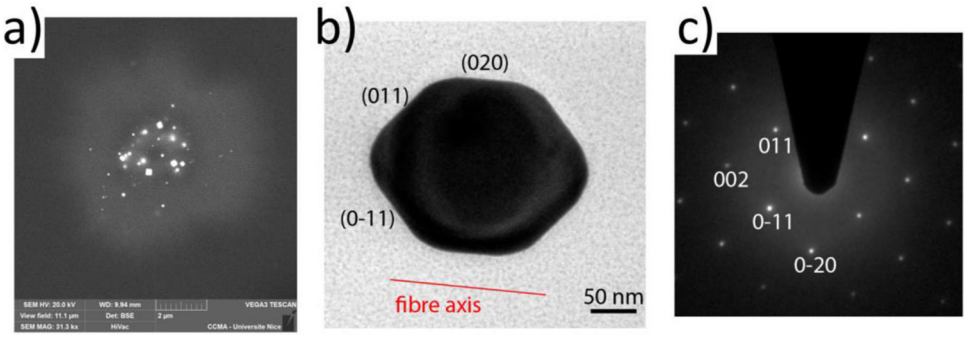

Fig. 11 Optical fiber containing $YbPO_4$ nanocrystals. **a** SEM image of the fiber core, **b** TEM image of the $YbPO_4$ crystals in < 100 > zone axis and **c** the corresponding SAED pattern. Images reprinted from Ref. [79], copyright 2023, with permission from Elsevier

nanoparticles [76]. As-prepared NPs are Boehmite (AlOOH) which are converted to alumina upon heat-treatment during the MCVD process. The reactivity of nanoparticles with the host glass can be a limitation to the choice of compositions. For example, YAG nanoparticles ($Y_3Al_5O_{12}$) dissolve during the manufacturing process, ultimately yielding YPO_4 nanoparticles through recombination with phosphorus from the core layer [77]. Fluoride nanoparticles (CaF_2, SrF_2, BaF_2, LaF_3) are also highly reactive with the silica matrix, leading to evaporation of fluorine in SiF_4 form from 1000 °C [78]. In contrast, $YbPO_4$ nanocrystals have been shown to survive all along the MCVD process and the drawing step [79]. Another manufacturing process is based on the direct doping method. In this method used to prepare mono-index fibers, the crystals are dispersed in the melted glass [80]. Using this technique, it was possible to prepare tellurite optical fibers doped with nanodiamonds (the nanodiamonds survival was estimated to be 1–6%) [81] and $LiYF_4$:Er^{3+},Yb^{3+} nanocrystals [82] or $SrAl_2O_4$:Eu^{2+},Dy^{3+} microparticles in phophate fibers [83].

The third approach is to obtain nanoparticles directly during the manufacturing process [49]. This method relies on thermodynamic phase separation mechanisms. Alkaline earth ions (Mg^{2+}, Sr^{2+}, Ca^{2+}) or La^{3+} are added to the silica during solution doping step [84–87]. The temperature involved in the MCVD process (up to ~ 2200°C) causes the glass to demix into two phases, one rich in silica and the other rich in phase-separating elements forming the nanoparticles. Such nanoparticles are silicates [60]. When rare-earths ions (Er^{3+}, Eu^{3+}, etc.) are added during solution doping, these ions are preferentially segregated in the nanoparticles, enabling them to increase their coordination number and favoring the change of their luminescence properties [60, 88]. The particles thus formed in preform are generally amorphous and spherical. Particle size is influenced by the concentration of phase-separating elements [46]. A broad size distribution is generally obtained. Spinodal morphology (interconnected phases) has only been reported once in fibers [89]. When preforms are drawn into optical fibers, the particles may decrease in size or undergo a change in shape, becoming elongated (Fig. 12) [90–92]. These elongated particles may fragment into daughter spherical particles via the formation of Rayleigh-Plateau instabilities. Drawing conditions (temperature, speed) are therefore very important to control in order to adjust the final characteristics of the particles in the fiber. Finally, the current use of Rayleigh-Plateau instabilities brings us back to the history of optical fibers, when Jean Daniel Colladon discovered light fountains and wanted to present recent discoveries on the instabilities of a jet of water (lately known as Rayleigh-Plateau instability).

5 Conclusions and future opportunities

This article allowed to provide insights into the long history of glass photonics. From its earliest uses, glass has been exploited for its unique optical properties, from its transparency to its ability to refract light. Glass has thus been a very important material for understanding the nature of light (e.g., the prism used by Sir I. Newton). In addition, photonic applications have led us to develop

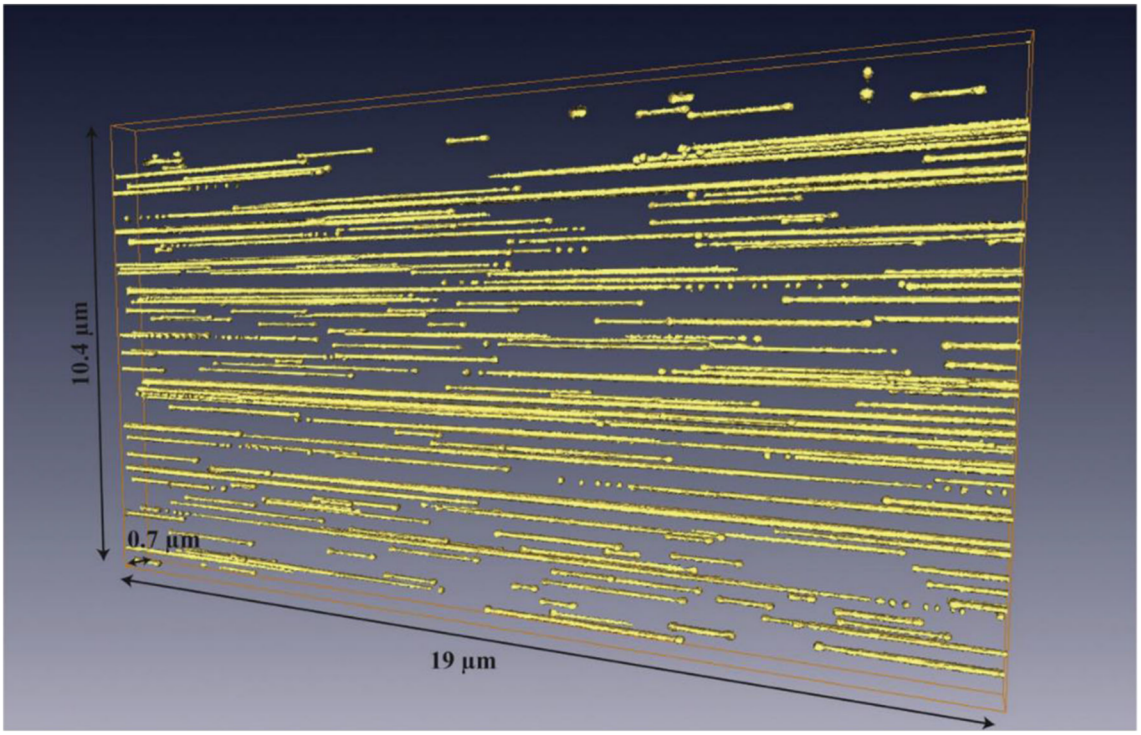

Fig. 12. 3D rendering of elongated particles in the fiber core. Smaller spherical particles, randomly distributed, are not represented. The drawing axis is horizontal. Images reprinted from Ref. [92], copyright 2021, with permission from Elsevier

our knowledge of glass to make it compatible with the intended applications (e.g., more transparent glass for optical fibers). Thus, the foundation of the marriage between glass and light lies on the triptych glass composition-glass structure-optical properties.

Future developments in glass photonics will be based on new tools such as machine learning and 3D printing. Machine learning and artificial intelligence should (1) help to predict new optical properties (luminescence, nonlinearity, transmission window, dispersion relation, etc.), (2) to determine new waveguide geometries and (3) to improve our ability to analyze optical signals to enhance sensor performance, for example. 3D printing and additive manufacturing will make it possible to (1) prepare waveguides with exotic geometries impracticable with the current manufacturing process, (2) to grow additional glass components on waveguides, and (3) to push hybrid integration with metals, semiconductors, organic materials, etc. Finally, the future of glass photonics may also depend on our ability to meet current challenges such as climate change, i.e., the development of an environmentally-friendly manufacturing process, considering environmental impact and possible material shortages.

Acknowledgements Financial support is grateful acknowledged from these supporters: CNRS and ANR (WB), the J. E. Sirrine Foundation (JB).

Declarations

Conflict of interest Authors are required to disclose financial or non-financial interests that are directly or indirectly related to the work submitted for publication. Please refer to "Competing Interests and Funding" below for more information on how to complete this section.

Data Availability Statement No Data associated in the manuscript.

References

1. D.L. Morse, J.W. Evenson, Int. J. Appl. Glass Sci. **7**, 409 (2016). https://doi.org/10.1111/ijag.12242
2. J. Ballato, *Opt. Photon. News* 31 (2022).
3. J. Ballato, Bull. Am. Ceram. Soc. **101**, 6 (2022)
4. P.D. Dragic, J. Ballato, Opt. Photon. News **25**, 44 (2014)
5. E. Snitzer, Phys. Rev. Lett. **7**, 444 (1961). https://doi.org/10.1103/PhysRevLett.7.444
6. C.J. Koester, E. Snitzer, Appl. Opt. **3**, 1182 (1964). https://doi.org/10.1364/AO.3.001182
7. K.C. Kao, G.A. Hockham, Proc. IEE. **133**, 1151 (1966). https://doi.org/10.1049/piee.1966.0189
8. F. Kapron, D. Keck, R. Maurer, Appl. Phys. Lett. **17**, 423 (1970). https://doi.org/10.1063/1.1653255

9. W. Blanc, Y.G. Choi, X. Zhang, M. Nalin, K.A. Richardson, G.C. Righini, M. Ferrari, A. Jha, J. Massera, S. Jiang, J. Ballato, L. Petit, Prog. Mater. Sci. **134**, 10108 (2023). https://doi.org/10.1016/j.pmatsci.2023.101084
10. J.D. Colladon, CR Acad. Sci. **15**, 800 (1842)
11. A. Ghatak, K. Thyagarajan, *An Introduction to Fiber Optics* (Cambridge University Press, Cambridge, 1998)
12. M.S. Islam, C.M. Cordeiro, M.A. Franco, J. Sultana, A.L. Cruz, D. Abbott, Opt. Express **28**, 16089 (2020). https://doi.org/10.1364/OE.389999
13. B.J. Eggleton, C. Kerbage, P.S. Westbrook, R.S. Windeler, A. Hale, Opt. Express **9**, 698 (2001). https://doi.org/10.1364/OE.9.000698
14. P. Russell, Science **299**, 358 (2003). https://doi.org/10.1126/science.1079280
15. A. Mafi, Adv. Opt. Photon. **7**, 459 (2015). https://doi.org/10.1364/AOP.7.000459
16. S. Karbasi, T. Hawkins, J. Ballato, K.W. Koch, A. Mafi, Opt. Mat. Express **2**, 1496 (2012). https://doi.org/10.1364/OME.2.001496
17. G.C. Righini, M. Ferrari, *Integrated Optics* (The Institution of Engineering and Technology, New York, 2021)
18. T. Otabara, J. Tatebayashi, T. Yoshimura, D. Timmerman, S. Ichikawa, Y. Fujiwara, Jpn. J. Appl. Phys. **62**, 1018 (2023). https://doi.org/10.35848/1347-4065/acbb0f
19. N. Yokoyama, R. Tanabe, Y. Yasuda, H. Honda, S. Ichikawa, Y. Fujiwara, T. Hikosaka, M. Uemukai, T. Tanikawa, R. Katayama, Jpn. J. Appl. Phys. **61**, 050902 (2022). https://doi.org/10.35848/1347-4065/ac57ab
20. E. Desurvire, *Erbium-Doped Fiber Amplifiers, Principles and Applications* (Wiley, New York, 1994)
21. M.J.F. Digonnet, *Rare-Earth-Doped Fiber Lasers and Amplifiers* (Marcel Dekker Inc, New York, 2001)
22. M. Ferrari, G.C. Righini, *Physics and Chemistry of Rare-Earth Ions Doped Glasses* (Trans Tech Publishers, New York, 2008)
23. A. Lukowiak, A. Chiasera, A. Chiappini, G.C. Righini, M. Ferrari, *Handbook of Sol-Gel Science and Technology* (Springer, Cham, 2017). https://doi.org/10.1007/978-3-319-19454-7_48-1
24. G.C. Righini, C. Armellini, M. Ferrari, A. Carlotto, A. Carpentiero, A. Chiappini, A. Chiasera, A. Lukowiak, T.N.L. Tran, S. Varas, Materials **16**, 2724 (2023). https://doi.org/10.3390/ma16072724
25. A. de Pablos-Martin, M. Ferrari, M.J. Pascual, G.C. Righini, La Rivista del Nuovo Cimento **38**, 311 (2015). https://doi.org/10.1393/ncr/i2015-10114-0
26. A. Chiappini, A. Chiasera, C. Armellini, S. Varas, A. Carpentiero, M. Mazzola, E. Moser, S. Berneschi, G.C. Righini, M. Ferrari, J. Sol-Gel Sci. Technol. **60**, 408 (2011). https://doi.org/10.1007/s10971-011-2556-y
27. T.N.L. Tran, A. Szczurek, A. Carlotto, S. Varas, G.C. Righini, M. Ferrari, J. Krzak, A. Lukowiak, A. Chiasera, Opt. Mater. **130**, 112577 (2022). https://doi.org/10.1016/j.optmat.2022.112577
28. S.J.L. Ribeiro, Y. Messaddeq, R.R. Gonçalves, M. Ferrari, M. Montagna, M.A. Aegerter, Appl. Phys. Lett. **77**, 3502 (2000). https://doi.org/10.1063/1.1329159
29. R.R. Gonçalves, G. Carturan, L. Zampedri, M. Ferrari, M. Montagna, A. Chiasera, G.C. Righini, S. Pelli, S.J.L. Ribeiro, Y. Messaddeq, Appl. Phys. Lett. **81**, 28 (2002). https://doi.org/10.1063/1.1489477
30. A. Peled, A. Chiasera, M. Nathan, M. Ferrari, S. Ruschin, Appl. Phys. Lett. **92**, 221104 (2008). https://doi.org/10.1063/1.2936961
31. L. Zur, L.T.N. Tran, M. Meneghetti, T.T.V. Tran, A. Lukowiak, A. Chiasera, D. Zonta, M. Ferrari, G.C. Righini, Opt. Mater. **63**, 95 (2008). https://doi.org/10.1016/j.optmat.2016.08.041
32. L.T.N Tran, C. Armellini, R. Balda, M. Benabdesselam, S. Berneschi , W. Blanc, B. Boulard, A. Carpentiero, A. Chiappini, A. Chiasera, P. Dentella, D. Dorosz, S. Eaton, M.C. Falconi, J. Fernandez, M. Ferrari, J. Gates, P. Gluchowski, G. Ischia, A. Lukowiak, F. Mady, D. Massella, G. Nunzi Conti, F. Prudenzano, B. Rossi, R. Ramponi, G.C. Righini, P.-J. Sazio, G. Speranza, S. Varas, D. Zonta, L. Zur, Proc. SPIE 11276, 1127614 (2020). https://doi.org/10.1117/12.2547526
33. "FLEXIBLE PHOTONICS: a multidisciplinary tool enabling sustainable development" https://www.sciencedirect.com/journal/optical-materials/special-issue/10LJ4J18H61
34. A.C.S. Van Heel, Nature **173**, 39 (1954). https://doi.org/10.1038/173039a0
35. H.H. Hopkins, N.S. Kapany, Nature **173**, 39 (1954). https://doi.org/10.1038/173039b0
36. Z.I. Alferov, Rev. Mod. Phys. **73**, 767 (2001). https://doi.org/10.1103/RevModPhys.73.767
37. https://www.youtube.com/watch?v=g9BL7vUjUfU
38. J. Hecht, *City of Light: The Story of Fiber Optics* (Oxford University Press on Demand, Oxford, 2004)
39. J. Ballato, P. Dragic, Int. J. Appl. Glass Sci. **7**, 413 (2016). https://doi.org/10.1111/ijag.12239
40. T. Li, *Optical Fiber Communications: Fiber Fabrication* (Elsevier, New York, 2012)
41. T. Hasegawa, Y. Tamura, H. Sakuma, Y. Kawaguchi, Y. Yamamoto, Y. Koyano, SEI Tech. Rev **86**, 18 (2018)
42. M. Poulain, J. Non-Cryst, Sol. **56**, 1 (1983). https://doi.org/10.1016/0022-3093(83)90439-8
43. M. Poulain, S. Cozic, J.L. Adam, *Mid-Infrared Fiber Photonics* (Woodhead Publishing, New York, 2022), pp.47–109
44. I. Cozmuta, D.J. Rasky, New Space **5**, 121 (2017). https://doi.org/10.1089/space.2017.0016
45. P. Tandon, M.J. Li, D.C. Bookbinder, S.L. Logunov, E.J. Fewkes, Nanophotonics **2**, 383 (2013). https://doi.org/10.1515/nanoph-2013-0032
46. W. Blanc, Z. Lu, T. Robine, F. Pigeonneau, C. Molardi, D. Tosi, Opt. Mat. Express **12**, 2635 (2022). https://doi.org/10.1364/OME.462822
47. A. Veber, Z. Lu, M. Vermillac, F. Pigeonneau, W. Blanc, L. Petit, Fibers **7**, 105 (2019). https://doi.org/10.3390/fib7120105
48. G. Liu, B. Jacquier, *Spectroscopic Properties of Rare Earths in Optical Materials* (Springer, Berlin, 2006)
49. W. Blanc, V. Mauroy, L. Nguyen, B.N. ShivakiranBhaktha, P. Sebbah, B.P. Pal, B. Dussardier, J. Am. Ceram. Soc. **94**, 2315 (2011). https://doi.org/10.1111/j.1551-2916.2011.04672.x
50. C. Kucera, B. Kokuoz, D. Edmondson, D. Griese, M. Miller, A. James, W. Baker, J. Ballato, Opt. Lett. **34**, 2339 (2009). https://doi.org/10.1364/OL.34.002339
51. T. Lindstrom, E. Garber, D. Edmonson, T. Hawkins, Y. Chen, G. Turri, M. Bass, J. Ballato, Opt. Mater Express. **2**, 1520 (2012). https://doi.org/10.1364/OME.2.001520
52. M. Vermillac, H. Fneich, J.F. Lupi, J.B. Tissot, C. Kucera, P. Vennéguès, A. Mehdi, D.R. Neuville, J. Ballato, W. Blanc, Opt. Mater. **68**, 24 (2017). https://doi.org/10.1016/j.optmat.2016.11.042
53. B.N. Samson, P.A. Tick, N.F. Borrelli, Opt. Lett. **26**, 145 (2001). https://doi.org/10.1364/OL.26.000145
54. K.E. Downey, B.N Samson, G.H. Beall, E.J. Mozdy, L.R. Pinckney, N.F. Borrelli, A. Mayolet, A. Kerdoncuff, C. Pierron, in *Conference on Lasers and Electro-Optics (CLEO)*, p. CTuP1 (2001)
55. B.N. Samson, L.R. Pinckney, J. Wang, G.H. Beall, N.F. Borrelli, Opt. Lett. **27**, 1309 (2002). https://doi.org/10.1364/OL.27.001309
56. C.C. Baker, E.J. Friebele, A.A. Burdett, D.L. Rhonehouse, J. Fontana, W. Kim, S.R. Bowman, L.B. Shaw, J. Sanghera, J. Zhang, R. Pattnaik, M. Dubinskii, J. Ballato, C. Kucera, A. Vargas, A. Hemming, N. Simakov, J. Haub, Opt. Express. **25**, 13903 (2017). https://doi.org/10.1364/OE.25.013903
57. P.A. Tick, Opt. Lett. **23**, 1904 (1998). https://doi.org/10.1364/OL.23.001904
58. R.W. Hopper, J. Non-Cryst, Solids **70**, 111 (1985). https://doi.org/10.1016/0022-3093(85)90098-5
59. A. Ishimaru, Y. Kuga, J. Opt. Soc. Am. **72**, 1317 (1982). https://doi.org/10.1364/JOSA.72.001317

60. W. Blanc, M.H.F. Francois-Saint-Cyr, X. Bidault, S. Chaussedent, C. Hombourger, S. Lacomme, P. Le Coustumer, D.R. Neuville, D.J. Larson, T.J. Prosa, C. Guillermier, J. Phys. Chem. C **123**, 29008 (2019)
61. J. Fourmont, W. Blanc, D. Guichaoua, S. Chaussedent, Sci. Rep. **12**, 11959 (2022). https://doi.org/10.1038/s41598-022-16139-w
62. S. Marzhan, S. Korganbayev, W. Blanc, T. Ayupova, A. Bekmurzayeva, M. Shaimerdenova, K. Dukenbayev, C. Molardi, D. Tosi, Opt. Lett. **43**, 5945 (2018). https://doi.org/10.1364/OL.43.005945
63. D. Tosi, C. Molardi, M. Sypabekova, W. Blanc, IEEE Sens. J. **21**, 12667 (2020). https://doi.org/10.1109/JSEN.2020.3010572
64. A. Beisenova, A. Issatayeva, Z. Ashikbayeva, M. Jelbuldina, A. Aitkulov, V. Inglezakis, W. Blanc, P. Saccomandi, C. Molardi, D. Tosi, Sensors **21**, 828 (2021). https://doi.org/10.3390/s21030828
65. A. Beisenova, A. Issatayeva, S. Sovetov, S. Korganbayev, M. Jelbuldina, Z. Ashikbayeva, W. Blanc, E. Schena, S. Sales, C. Molardi, D. Tosi, Biomed. Opt. Express **10**, 1282 (2019). https://doi.org/10.1364/BOE.10.001282
66. Z. Ashikbayeva, A. Aitkulov, M. Jelbuldina, A. Issatayeva, A. Beisenova, C. Molardi, P. Saccomandi, W. Blanc, V.J. Inglezakis, D. Tosi, Sci. Rep. **10**, 12593 (2020). https://doi.org/10.1038/s41598-020-69384-2
67. A. Amantayeva, N. Adilzhanova, A. Issatayeva, W. Blanc, C. Molardi, D. Tosi, Biosensors **11**, 446 (2021). https://doi.org/10.3390/bios11110446
68. A. Issatayeva, A. Amantayeva, W. Blanc, D. Tosi, C. Molardi, Sci. Rep. **11**, 8609 (2021). https://doi.org/10.1038/s41598-021-88117-7
69. A. Aitkulov, M. Sypabekova, C. Molardi, W. Blanc, D. Tosi, Measurement **172**, 108874 (2021). https://doi.org/10.1016/j.measurement.2020.108874
70. M. Sypabekova, A. Aitkulov, W. Blanc, D. Tosi, Biosens. Bioelectron. **165**, 112365 (2020). https://doi.org/10.1016/j.bios.2020.112365
71. M. Olivero, A. Mirigaldi, V. Serafini, A. Vallan, G. Perrone, W. Blanc, M. Benabdesselam, F. Mady, C. Molardi, D. Tosi, E.E.E. Trans, Instrum. Meas. **70**, 1 (2021). https://doi.org/10.1109/TIM.2021.3075518
72. M. Silveira, A. Frizera, A. Leal-Junior, D. Ribeiro, C. Marques, W. Blanc, C.A. Diaz, Opt. Fiber Technol. **58**, 102303 (2020). https://doi.org/10.1016/j.yofte.2020.102303
73. A.G. Leal-Junior, D. Ribeiro, L.M. Avellar, M. Silveira, C.A.R. Díaz, A. Frizera-Neto, W. Blanc, E. Rocon, C. Marques, IEEE Sens. J. **21**, 2995 (2020). https://doi.org/10.1109/JSEN.2020.3024242
74. L. Avellar, A. Frizera, H. Rocha, M. Silveira, C. Díaz, W. Blanc, C. Marques, A. Leal-Junior, Phot. Res. **11**, 364 (2023). https://doi.org/10.1364/PRJ.471301
75. J. Luo, X. Zhang, S. Yang, W. Blanc, Z. Yan, X. Yu, I.E.E.E. Phot, Technol. Lett. **35**, 613 (2023). https://doi.org/10.1109/LPT.2023.3264576
76. A. Le Sauze, C. Simonneau, A. Pastouret, D. Gicquel, L. Bigot, S. Choblet, A.M. Jurdyc, B. Jacquier, D. Bayart, L. Gasca, in *Optical Amplifiers and Their Applications*, p. WC5. (2003)
77. V. Fuertes, N. Grégoire, P. Labranche, S. Gagnon, N. Hamada, B. Bellanger, Y. Ledemi, S. LaRochelle, Y. Messaddeq, ACS Appl. Nano Mater. **6**, 4337 (2023). https://doi.org/10.1021/acsanm.2c05449
78. H. Fneich, M. Vermillac, D.R. Neuville, W. Blanc, A. Mehdi, Ceramics **5**, 182 (2022). https://doi.org/10.3390/ceramics5020016
79. Z. Lu, N. Vakula, M. Ude, M. Cabié, T. Neisius, F. Orange, F. Pigeonneau, L. Petit, W. Blanc, Opt. Mater. **138**, 113644 (2023). https://doi.org/10.1016/j.optmat.2023.113644
80. N. Ojha, M. Tuomisto, M. Lastusaari, L. Petit, RSC Adv. **8**, 19226 (2018). https://doi.org/10.1039/C8RA03298J
81. M. Henderson, B. Gibson, H. Ebendorff-Heidepriem, K. Kuan, S.V. Afshar, J. Orwa, I. Aharonovich, S. Tomljenovic-Hanic, A. Greentree, S. Prawer, T. Monro, Adv. Mater. **23**, 2806 (2011). https://doi.org/10.1002/adma.201100151
82. J. Zhao, X. Zheng, E.P. Schartner, P. Ionescu, R. Zhang, T.L. Nguyen, D. Jin, H. Ebendorff-Heidepriem, Adv. Opt. Mat. **4**, 1507 (2016). https://doi.org/10.1002/adom.201600296
83. A. Lemiere, A. Szczodra, S. Vuori, B. Bondzior, T.W. Hawkins, J. Ballato, M. Lastusaari, J. Massera, L. Petit, Mater. Res. Bull. **153**, 111899 (2022). https://doi.org/10.1016/j.materresbull.2022.111899
84. W. Blanc, V. Mauroy, B. Dussardier, Int. J. Nanotechnol. **9**, 480 (2012). https://doi.org/10.1504/IJNT.2012.045350
85. M. Vermillac, H. Fneich, J. Turlier, M. Cabié, C. Kucera, D. Borschneck, F. Peters, P. Vennéguès, T. Neisius, S. Chaussedent, D.R. Neuville, W. Blanc, Opt. Mater. **87**, 74 (2019). https://doi.org/10.1016/j.optmat.2018.05.067
86. V. Fuertes, N. Grégoire, P. Labranche, S. Gagnon, V.A.G. Rivera, S. LaRochelle, Y. Messaddeq, J. Alloys Compd. **17**, 168928 (2023). https://doi.org/10.1016/j.jallcom.2023.168928
87. V. Fuertes, N. Grégoire, S. Morency, S. Gagnon, Y. Ledemi, S. LaRochelle, Y. Messaddeq, Opt. Mater. Express **12**, 1323 (2022). https://doi.org/10.1364/OME.451311
88. J. Turlier, J. Fourmont, X. Bidault, W. Blanc, S. Chaussedent, Ceram. Int. **46**, 26264 (2020). https://doi.org/10.1016/j.ceramint.2020.03.293
89. M. Cavillon, B. Faugas, J. Zhao, C. Kucera, B. Kukuoz, P. Dragic, X. Qiao, J. Du, J. Ballato, J. Chem. Therm. **128**, 119 (2019). https://doi.org/10.1016/j.jct.2018.08.016
90. M. Vermillac, J.-F. Lupi, F. Peters, M. Cabié, P. Vennegues, C. Kucera, T. Neisius, J. Ballato, W. Blanc, J. Am. Ceram. Soc. **100**, 1814 (2017). https://doi.org/10.1111/jace.14774
91. V. Fuertes, N. Grégoire, P. Labranche, S. Gagnon, R. Wang, Y. Ledemi, S. LaRochelle, Y. Messaddeq, Sci. Rep. **11**, 1 (2021). https://doi.org/10.1038/s41598-021-88572-2
92. M. Cabié, T. Neisius, W. Blanc, Mater. Charac. **178**, 111261 (2021). https://doi.org/10.1016/j.matchar.2021.111261